Beamforming Techniques for NOMA-based Integrated Sensing and Communication Systems

Chentong Li, Saeed Mohammadzadeh, *Member, IEEE,* Haitham Al-Obiedollah, *Member, IEEE,* Kanapathippillai Cumanan, *Senior Member, IEEE,* and Octavia A. Dobre, *Fellow, IEEE.*

***Abstract*—In this paper, beamforming techniques are proposed for an integrated sensing and communication (ISAC) system based on non-orthogonal multiple access (NOMA). Specifically, a multi-antenna dual-functional base station simultaneously performs target sensing and serves multiple single-antenna NOMA communication users. To investigate the potential capabilities of this NOMA-based ISAC system, we first develop a beamforming technique for the max-min signal-to-interference-and-noise ratio (SINR) balancing problem. However, the original form is not convex regarding the design parameters. We propose an iterative algorithm that uses a bisection search to address the non-convexity problem and achieve a feasible solution to the original SINR balancing problem. This approach involves solving an equivalent power minimization problem, where we exploit the semidefinite relaxation technique. We also consider a robust design for the power minimization problem by taking into account inevitable imperfect channel state information. The numerical results show that the proposed NOMA-based ISAC performs better than the conventional orthogonal multiple access-based ISAC system in terms of transmit power consumption and balanced SINR while meeting the quality of service requirements regardless of the uncertainty of the associated channel.**

***Index Terms*—Integrated Sensing and Communication, Non-Orthogonal Multiple Access, signal-to-interference-and-noise ratio balancing, and power minimization.**

I. Introduction

Future wireless communications systems, including sixth-generation (6G) and beyond, are expected to meet unprecedented requirements such as higher spectral and energy efficiency, massive connectivity to support smart cities and homes, and precise sensing capabilities for emerging novel applications [1]. In this context, sensing becomes increasingly important as it plays a key role in providing more information, such as location data from the environment cite I10. Therefore, advanced joint system design could integrate communication, sensing, control, and computation, which are being considered to support smart cities and other new applications of the Internet of Things (IoT) in 6G and beyond [1]. In line with this trend, the idea of an integrated sensing and communication (ISAC) system appears as a critical solution, integrating communication and radar sensing functions on a single platform to serve both communication users and sensing targets. By sharing the same spectrum, ISAC enhances resource efficiency while enabling sensing capabilities that support various IoT applications [1]. In fact, in an effort to smoothly integrate sensing and communication into a single system, ISAC systems are currently shifting toward the use of larger antenna arrays, operation at higher frequency bands, and increased miniaturization.

Another challenge that must be considered is the exponential growth of mobile users, and various IoT devices present a significant challenge to provide massive connectivity in 6G and beyond. However, existing designs from previous generations of wireless technology struggle to meet these stringent requirements. If we focus only on communicating users, traditional orthogonal multiple access (OMA) technology, such as TDMA, FDMA and OFDMA, which can allocate orthogonal time or frequency resources to each user, ensuring simple implementation, struggle to accommodate such a large number of users due to its limited degree of freedom (DoFs), limits spectral efficiency and user capacity [2]. To address this, non-orthogonal multiple access (NOMA) has been recommended as a feasible technique, which can transmit superposition coded (SC) signals and adopt successive interference cancellation (SIC) to introduce additional DoFs in the power domain, thereby facilitating non-orthogonal resource sharing among more users [2]. This can enhance DoFs for communication users while allowing the integration of sensing targets [3], [4].

In summary, NOMA provides efficient interference management and flexible resource allocation, which is suitable for integration with ISAC systems. First, NOMA enables simultaneous service to multiple communication users and sensing targets using shared beamforming resources, enhancing the use of limited beampattern. Second, the additional DoFs provided by NOMA improve system flexibility in managing trade-offs between sensing and communication performance. Third, incorporating NOMA into the foundational ISAC system can effectively support the massive number of users and sensing targets that are anticipated in the next generation of wireless networks. Hence, a NOMA-based ISAC (NOMA-ISAC) system is an ideal communication system where the complementary benefits of each technique are exploited. In addition, this enhances the system's capacity to accommodate a growing number of communication users while supporting sensing capabilities.

C. Li, S. Mohammadzadeh and K. Cumanan are with School of Physics Engineering and Technology, University of York, York, YO10 5DD, U.K. (email: cl2215@york.ac.uk; Saeed.mohammadzadeh@york.ac.uk; kanapathippillai.cumanan@york.ac.uk).

H. Al-Obiedollah is with the Department of Electrical Engineering, Faculty of Engineering, The Hashemite University, P.O. Box 330127, Zarqa 13133, Jordan. (email:haithamm@hu.edu.jo.)

O. A. Dobre is with the Department of Electrical and Computer Engineering, Memorial University, St. John's NL A1B, Canada (email:odobre@mun.ca).

The work of S. Mohammadzadeh and K. Cumanan were supported by the UK Engineering and Physical Sciences Research Council (EPSRC) under grant number EP/X01309X/1.

The work of O. A. Dobre was supported in part by the Canada Research Chairs Program CRC-2022-00187 and the NSERC Discovery grant RGPIN-2019-04123.

A. Prior and Related Works

Preceding the advent of the ISAC systems, substantial research efforts have been made over the past decade to coexist with various communication and sensing systems. Early developments in this area primarily explored the embedding of communication signals in radar waveforms, particularly to enhance the capabilities of military radar systems [1]. As multi-input multi-output (MIMO) technologies advanced, the focus gradually changed to using radar waveforms for data modulation, facilitating the simultaneous use of signals for both communication and sensing [5]–[7]. Moreover, orthogonal frequency division multiple access (OFDMA) inspired two designs to emerge: radar-centric (or sensing-centric) and communication-centric designs by modifying their original waveforms to serve both communication users and sensing targets simultaneously, and some technologies are independent of the underlying systems and signals [8]. The radar-centric design is suitable when high throughput is unnecessary, as communication assumes a secondary role. In contrast, communication-centric design tends to have high throughput to meet the communication requirement. Both designs attempt to exploit the strengths of one waveform to serve sensing targets and communication users and enhance overall functionality. However, a key limitation is that they tend to optimize one function at the expense of the other, resulting in suboptimal performance.

When it comes to high-frequency bands, massive MIMO (mmMIMO) radar and communication systems employ similar hardware infrastructures and share signal processing techniques, such as beamforming, resulting in significant overlap in their structural and functional designs [9], [10]. Hence, sensing capabilities are no longer confined to specialized radar equipment; rather, wireless communication systems and devices can now enable environmental sensing [1]. This convergence has driven the development of ISAC systems, where both functionalities operate within a unified framework through shared waveforms that simultaneously support sensing and communication.

This system that combines sensing and communication was known by a number of names, including radar-communication (RadCom) [11], [12] and joint radar and communication (JRC) [13]. RadCom systems, which exploit similar architectures and carrier frequencies, are effective for simultaneous data transmission and sensing, enabling communication and remote sensing [11], [12], [14]. JRC systems aim to balance radar and communication performance while mitigating interference, with multi-input multi-output (MIMO) integration identified as a key strategy to enhance interference reduction [8], [13], [15], [16]. Building on these works, the ISAC system proposes that communication and sensing services can use the same frequency band and technological device by designing a shared waveform, thereby enhancing spectrum efficiency and reducing hardware cost [17]. ISAC not only supports communication users but also performs sensing tasks such as positioning and tracking, enhancing applications such as smart cities and vehicle-to-everything (V2X) applications [1]. Furthermore, ISAC supports advanced applications, including advanced positioning and tracking, sensing-aided beam training, and resource allocation [17].

To improve the accuracy of the ISAC, the transmitter is designed to focus the power toward specific areas of interest, thereby achieving accurate target estimation while maintaining reliable service for communication users [17]. Hence, beamforming design has become an effective approach in ISAC systems to meet both communication and sensing requirements [18], [19]. This technology allows the transmitter to direct its energy toward specific communication users or targets, thereby improving signal strength and quality, reducing interference, and maximizing spectral efficiency; the shared spectrum could be considered for beamforming. The use of beamforming in ISAC systems can effectively allocate shared spectrum resources, ensuring robust performance for communication and sensing applications [14].

In addition to conventional approaches, emerging technologies such as machine learning offer significant potential for enhancing the performance of ISAC systems. Learning-based models can be trained to extract essential features from data and adapt efficiently to dynamic, real-time environments. For example, the study in [20] proposes an ISAC beamforming neural network based on unsupervised learning, demonstrating its potential to reduce computational complexity while preserving system performance. Similarly, the work in [21] considers an ISAC system which uses deep learning techniques to optimize the achievable sum-rate. Furthermore, [22] presents a model-driven ISAC system that improves both communication and sensing efficiency. In addition, [23] introduces an edge learning framework that supports the communication model and the sensing model, providing a promising foundation to solve ISAC-related problems. These studies highlight the applicability of machine learning techniques in ISAC and suggest that such methods can be leveraged further in NOMA-ISAC systems to improve overall performance and scalability.

However, the DoFs become greatly limited as the number of users and targets rises, particularly when their number exceeds the number of antennas, which poses a significant challenge to the ISAC system [18]. Therefore, NOMA has been introduced to provide additional DoFs to support a larger number of communication users and sensing targets.

NOMA is a future-oriented, efficient multiple-access technology due to its advantages in spectral and energy efficiency, fairness, and capacity to support massive connectivity. NOMA allows multiple communication users to share time-frequency resources simultaneously through multiplexing of the power domain, effectively improving the system's DoFs [24]. Specifically, the base station (BS) simultaneously transmits an SC signal to each NOMA receiver. Users with stronger channel conditions first decode the signals for the weaker users and apply SIC to subtract these signals from the SC transmission, then decode their own signals. Meanwhile, users with weaker channel conditions decode only their own signals, treating the signals of other users as interference, allowing them to be allocated more power [25]–[27]. This differentiation allows the system to exploit the varying channel conditions of the users, effectively increasing the DoFs, and the SIC could reduce interference between users. Compared to traditional OMA

techniques such as OFDMA, which allocate separate frequency resources to individual users, thus constraining spectral efficiency and limiting user capacity, NOMA presents several key advantages. By enabling simultaneous transmission over shared resources through advanced interference management and flexible resource allocation, NOMA enhances spectral and energy efficiencies, improves user fairness, and supports massive connectivity [28], [29]. These features make NOMA particularly well-suited for integration with ISAC systems in future wireless networks.

Therefore, we aim to develop a NOMA-based ISAC system, referred to as NOMA-ISAC, which combines NOMA and ISAC technologies. In this system, the BS simultaneously sends information to communication users and probing targets, and communication users exploit NOMA to improve both spectral and energy efficiencies. Therefore, the NOMA-ISAC system can effectively utilize limited DoFs to accommodate more communication users and ensure the sensing targets receive sufficient power to perform their functions by sharing the same beamforming and hardware platform with communication services.

Several studies have explored optimizing performance metrics in NOMA-ISAC systems. In [30], the authors propose uplink and downlink models for NOMA-ISAC, where the uplink design facilitates flexible resource allocation between the communication and sensing functions, and the downlink designs aim to reduce interference for inter-communication users and between communication users and sensing targets. The study in [31] solved the problem of minimizing transmit power while satisfying the probability constraints of outages of communication users and the target requirements. Similarly, [32] introduces a resource allocation technique to maximize weighted sum throughput while optimizing sensing power, while [33] demonstrates that the NOMA-ISAC framework can achieve an expanded rate region in both uplink and downlink transmissions, highlighting its efficiency in enhancing spectral utilization. Lastly, [34] investigates inter-user interference and suggests a two-stage SIC-based framework to manage interference between communication users and sensing targets.

B. Contributions and Notation

Motivated by the above-mentioned work, we investigate a downlink transmission in a NOMA-ISAC system and solve two resource allocation problems. The first is the max-min SINR balancing problem, where the minimum SINR of the users is maximized to maintain fairness between users. The second is the power minimization problem, where the total transmit power is minimized while satisfying the required quality of service. Specifically, we consider two scenarios for the power minimization problem: one with perfect channel state information (CSI) and the other with an imperfect CSI assumption. The key contributions and findings of the paper are outlined as follows:

- We introduce a basic NOMA-ISSAC system that is capable of transmitting communication and sensing signals simultaneously using shared beamforming resources and establishing performance metrics for each function.
- In order to maintain user fairness, we formulate a max-min SINR balancing problem for communication users within a total power constraint while guaranteeing sufficient power allocation for the sensing target. To address the non-convexity of the original problem, we consider an equivalent power minimization problem and employ an iterative bisection search, which is exploited to obtain near-optimal solutions, ensuring efficient resource allocation.
- For the non-convex power minimization problem, where aim to minimize the total transmit power while ensuring communication users meet their required SINR threshold and the sensing target receives sufficient power, we consider solving it through semidefinite relaxation (SDR) techniques under the perfect CSI assumption.
- Due to practical limitations, we also formulate a robust power minimization problem to mitigate the impact of channel uncertainties. Under the imperfect CSI, we adopt a worst-case robust optimization framework to show that robust design meets system requirements while guaranteeing that each communication user's and sensing target's service requirements are satisfied.

Overall, the performance of the NOMA-ISAC and OMA-ISAC systems is evaluated and compared based on numerical results. The results of the max-min SINR balancing problem indicate that the NOMA-ISAC system achieves a higher balanced SINR under total transmit power constraints. In the power minimization problem, the simulation results show that the NOMA-ISAC system meets the required SINR thresholds with less power consumption while ensuring sufficient power is allocated to the sensing targets. Additionally, the study also highlights that the NOMA-ISAC system outperforms the OMA-ISAC system in robust design scenarios, indicating its resilience to channel uncertainties.

The remainder of this paper is structured as follows. Section II introduces the system model of a NOMA-ISAC system and defines the constraints for communication users and sensing targets. Section III formulates the max-min SINR balancing problem for the NOMA-ISAC system under the perfect CSI, which is shown to be equivalent to a power minimization problem. Section IV extends the power minimization problem under the imperfect CSI, proposing a robust design to account for channel uncertainties. Section V presents the numerical results of the max-min SINR balancing problem, the power minimization problem under the perfect CSI assumption, and the robust designs under imperfect CSI. Finally, we conclude this paper in Section VI.

Notations: We use lowercase and uppercase boldface letters for vectors and matrices, respectively. $\mathbb{E}\{\cdot\}$ and $\Re\{\cdot\}$ stand for the statistical expectation of random variables and the real part of a complex number, respectively. The symbol $\mathbb{C}$ is used for the complex numbers of n-dimensions and $\mathbb{R}$ for the real numbers. $(\cdot)^H$ and $\mathrm{Tr}(\cdot)$ denote conjugate transpose and the trace of a matrix, respectively. The Euclidean norm of a matrix is denoted by $\|\cdot\|_2$. $\mathbf{B} \succeq 0$ indicates that $\mathbf{B}$ is a positive semidefinite matrix.

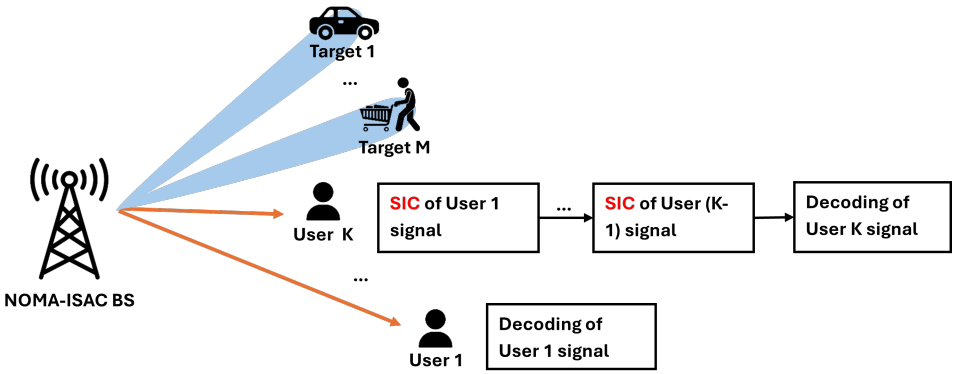

Fig. 1: Illustration of a downlink NOMA-ISAC system.

II. System Model

In this paper, we consider a NOMA-ISAC system, in which a dual-functional NOMA-ISAC BS equipped with N antennas communicates with K single-antenna communication users indexed by $\mathcal{K} \in \{1, \cdots, K\}$. Furthermore, the NOMA-ISAC BS serves M sensing targets indexed by $\mathcal{M} \in \{1, \cdots, M\}$ as shown in Fig. 1.

1) Communication Part: The BS in this system utilizes NOMA to send signals to all communication users at the same time using the beamformer $\mathbf{w}_k \in \mathbb{C}^{N\times 1}$ to deliver the symbol s_k, with s_k as the symbol intended for user k. We assumed $\mathbb{E}\{|s_k|^2\} = 1$. Hence, the received signal at user k is expected as:

$$y_k = \mathbf{h}_k^H \mathbf{w}_k s_k + \sum_{i=1,\, i\neq k}^{K} \mathbf{h}_k^H \mathbf{w}_i s_i + n_k, \tag{1}$$

where $\mathbf{h}_k \in \mathbb{C}^{N\times 1}$ represents the complex channel vector between user k and the BS, n_k stands for zero-mean circularly symmetric additive white Gaussian noise with variance σ_n^2.

Communication users are assumed to decode their messages based on their channel strength following the concept of NOMA, and the channel quality of communication users is ordered as $||\mathbf{h}_1||_2 \leq ||\mathbf{h}_2||_2 \leq \cdots \leq ||\mathbf{h}_K||_2$. Since NOMA could perform SIC on the communication user receiver to decode the corresponding signal, each user k can detect and remove the signal of the preceding $(k-1)$ users signals successively and treat the signal of the subsequent users $(k+1)$ to the user K as noise [35]. In order to identify user k, the remaining signal at user l is thus represented as follows:

$$y_l^k = \mathbf{h}_l^H \mathbf{w}_k s_k + \sum_{i=k+1}^{K} \mathbf{h}_l^H \mathbf{w}_i s_i + n. \tag{2}$$

To guarantee successful SIC implementation, higher power levels should be assigned to the weaker users; this can be achieved by satisfying the following constraints:

$$|\mathbf{h}_k^H \mathbf{w}_1|^2 \geq \cdots \geq |\mathbf{h}_k^H \mathbf{w}_{k-1}|^2 \geq |\mathbf{h}_k^H \mathbf{w}_k|^2 \geq |\mathbf{h}_k^H \mathbf{w}_{k+1}|^2 \geq \cdots \geq |\mathbf{h}_k^H \mathbf{w}_K|^2, \ \forall k \in \mathcal{K}. \tag{3}$$

Hence, user l decodes the message intended for user k with the following SINR:

$$\text{SINR}_l^k = \frac{|\mathbf{h}_l^H \mathbf{w}_k|^2}{\sum_{i=k+1}^{K} |\mathbf{h}_l^H \mathbf{w}_i|^2 + \sigma^2}. \tag{4}$$

2) Sensing Part: Since sensing targets share the same spectrum with communication users, the ISAC system beamformer can be used to detect targets. The beampattern gain of the detection signal $P(\theta_m)$ is directed towards the target's direction when the system is operating in tracking mode, and there is previously detected information about the target [36]. Hence the beampattern gain $P(\theta_m)$ is given by:

$$P(\theta_m) = \boldsymbol{\alpha}^H(\theta_m) \mathbf{R}_c \boldsymbol{\alpha}(\theta_m), \tag{5}$$

where $\theta_m, \forall m \in \mathcal{M}$ denotes the direction of the target. The corresponding steering vector is expressed as $\boldsymbol{\alpha}(\theta_m) = [1, e^{j\frac{2\pi}{\lambda} d \sin(\theta_m)}, \ldots, e^{j\frac{2\pi}{\lambda} d(N-1)\sin(\theta_m)}]^T$, where λ represent the carrier wavelength, and $d \leq (\lambda/2)$ indicates the antenna spacing, respectively. Moreover, $\mathbf{R}_c$ is the covariance matrix of the transmit signal for sensing user defined as [32]:

$$\mathbf{R}_c = \sum_{k=1}^{K} \mathbf{w}_k \mathbf{w}_k^H. \tag{6}$$

Meanwhile, in order to ensure good sensing quality, the cross-correlation between transmitted signals at a given target location should be as low as possible [36]. Thus, for any two sensing targets directions θ_p and θ_m, the cross-correlation is denoted as $C(\theta_p, \theta_m) = |\boldsymbol{\alpha}^H(\theta_p) \mathbf{R}_c \boldsymbol{\alpha}(\theta_m)|^2, \forall p \neq m \in \mathcal{M}$, while the mean-squared cross-correlation of $\frac{M^2-M}{2}$ pairs of the sensing users is given as:

$$\overline{C} = \frac{2}{M^2 - M} \sum_{p=1}^{M-1} \sum_{m=p+1}^{M} C(\theta_p, \theta_m). \tag{7}$$

III. Max-min SINR Problem for NOMA-ISAC System

In this section, we examine the problem of maximizing the minimum achievable SINR of communication users under a given total power constraint (max-min SINR) while ensuring

sufficient power allocation to the sensing targets under the perfect CSI. Since the NOMA technique allows for more flexible management of communication users, it may be more efficient to offer a fair SINR performance across the communication users. Additionally, in the NOMA-ISAC system, the power threshold required for sensing targets must be incorporated into the design. Therefore, the problem is defined as:

$$\begin{aligned}
&\max \min_{l\in\{k,k+1,\cdots,K\}} \text{SINR}_l^k \\
&\text{s.t.} \sum_{k=1}^{K} \|\mathbf{w}_k\|_2^2 \le P_{\text{total}}, && \text{(8a)}\\
&\quad P(\theta_m) \ge P_s,\ \forall m \in \mathcal{M}, && \text{(8b)}\\
&\quad |P(\theta_p) - P(\theta_m)| \le P_{\text{diff}},\ \forall p \ne m \in \mathcal{M}, && \text{(8c)}\\
&\quad \overline{C} \le \xi, && \text{(8d)}
\end{aligned}$$

where $\|\mathbf{w}_k\|_2^2$ denote the power of the k^{th} communication user. The P_{total} represents the total transmit power available at the BS. The constraint (8a) ensures that the total power of the communication users is below the available power threshold. Furthermore, P_s represents the minimum sensing threshold, and constraint (8b) specifies that the power allocated to each sensing target must be higher than the respective power threshold. Moreover, (8c) ensures that the power difference between two sensing targets remains less than the predefined threshold P_{diff}. Finally, an upper bound of the mean-squared cross-correlation is guaranteed by (8d).

However, the max-min problem is inherently non-convex, and the constraints in (8c) are also non-convex due to the quadratic structure of the covariance matrix, making the optimization problem (8) challenging to solve directly. In order to address this issue, we utilize the bisection method and introduce a slack variable t, representing the minimum SINR for all communication users, which we maximize. Consequently, (8) can be changed as follows:

$$\begin{aligned}
&\max\ \ t \\
&\text{s.t.}\ \ \text{SINR}_l^k \ge t,\ \forall k \in \mathcal{K}, \\
&\qquad \text{(8a)} - \text{(8d)}.
\end{aligned} \tag{9}$$

Let t^{opt} represent the optimal solution for (9). If $t \ge t^{\text{opt}}$, (9) becomes infeasible; conversely, if $t \le t^{\text{opt}}$, (9) is feasible. Therefore, (9) is transformed into a feasible problem that aims to find a set of $\mathbf{w} = \{\mathbf{w}_1, \cdots, \mathbf{w}_K\}$ that satisfies all constraints for a given value t. This reformulation enables the application of a bisection method to solve the problem, which efficiently narrows the feasible range until it converges to the specified threshold, reducing the result value toward the global optimal value. By selecting t through the bisection method, the solution is achieved by solving the following problem:

$$\begin{aligned}
&\min_{\mathbf{w}_k\in\mathbb{C}^{N\times 1}} \sum_{k=1}^{K} \|\mathbf{w}_k\|_2^2 \\
&\text{s.t. } \text{SINR}_l^k \ge t,\ \forall k \in \mathcal{K} \\
&\qquad \text{(8a)} - \text{(8d)}.
\end{aligned} \tag{10}$$

Here, (10) is equivalent to minimizing total transmit power while ensuring that communication users achieve the desired SINR threshold and the sensing target receives sufficient power. To determine a feasible solution for (10), we introduce the new matrix $\mathbf{W}_k = \mathbf{w}_k\mathbf{w}_k^H$ and $\mathbf{H}_k = \mathbf{h}_k\mathbf{h}_k^H$, and follow the trace rule $\mathbf{w}^H\mathbf{H}\mathbf{w} = \text{Tr}(\mathbf{H}\mathbf{w}\mathbf{w}^H) = \text{Tr}(\mathbf{H}\mathbf{W})$. In addition, we define a matrix $\mathbf{A}_m = \boldsymbol{\alpha}(\theta_m)\boldsymbol{\alpha}^H(\theta_m)$. Next, using the new matrices $\mathbf{W}_k$, $\mathbf{H}_k$ and $\mathbf{A}_m$, we can express the power $P(\theta_m)$ in (5) as:

$$\begin{aligned}
P(\theta_m) &= \boldsymbol{\alpha}^H(\theta_m)\mathbf{R}_c\boldsymbol{\alpha}(\theta_m) = \text{Tr}(\mathbf{R}_c\boldsymbol{\alpha}(\theta_m)\boldsymbol{\alpha}^H(\theta_m)) \\
&= \text{Tr}(\mathbf{A}_m\mathbf{R}_c) = \sum_{k=1}^{K} \text{Tr}(\mathbf{A}_m\mathbf{W}_k),\ \forall m \in \mathcal{M}.
\end{aligned} \tag{11}$$

Hence, the problem (10) can be rewritten as follows:

$$\begin{aligned}
&\min_{\mathbf{W}\in\mathbb{C}^{N\times N}} \sum_{k=1}^{K} \text{Tr}(\mathbf{W}_k) \\
&\text{s.t. } \text{Tr}(\mathbf{H}_l\mathbf{W}_k) - t\Big(\sum_{i=k+1}^{K} \text{Tr}(\mathbf{H}_l\mathbf{W}_i) + \sigma_n^2\Big) \ge 0, \\
&\qquad\qquad \forall k \in \mathcal{K},\ l = k, k+1, \cdots, K, && \text{(12a)}\\
&\quad \mathbf{W}_k = \mathbf{W}_k^H,\ \mathbf{W}_k \succeq 0, && \text{(12b)}\\
&\quad \text{rank}(\mathbf{W}_k) = 1, && \text{(12c)}\\
&\quad \sum_{k=1}^{K} \text{Tr}(\mathbf{W}_k) \le P_{\text{total}}, && \text{(12d)}\\
&\quad \sum_{k=1}^{K} \text{Tr}(\mathbf{A}_m\mathbf{W}_k) \ge P_s,\ \forall m \in \mathcal{M}, && \text{(12e)}\\
&\quad \Big|\sum_{k=1}^{K} \text{Tr}((\mathbf{A}_p - \mathbf{A}_m)\mathbf{W}_k)\Big| \le P_{\text{diff}},\ \forall p \ne m \in \mathcal{M}, && \text{(12f)}\\
&\quad \overline{C} \le \xi. && \text{(12g)}
\end{aligned}$$

The optimization problem described in (12) remains non-convex because of the non-convex rank-one constraints in (12c). Hence, we reformulate (12) as a standard semidefinite programming (SDP) problem by applying semidefinite relaxation (SDR), where the rank-one constraint is relaxed. This relaxation transforms the original non-convex problem into a convex SDP, whose solution provides a lower bound to the original problem [37]. According to established results in SDR theory, relaxation is often tight, which means that the relaxed problem's optimal solution remains rank-one [38]. A formal proof for this tightness is provided in Appendix A.

Based on this reformulation, we can determine a suitable solution for the equivalent power minimization problem and apply a bisection search to solve the original max-min SINR problem. The algorithm for determining the optimal value is summarized in Algorithm 1.

Specifically, to confirm that the relaxation in problem (13) is tight, we verify that the optimal solution $\mathbf{W}^{\text{opt}}$ satisfies the rank-one constraint, even though it was relaxed during formulation, indicating that the relaxation is tight. Hence, a set of rank-one $\mathbf{W}_k$ is obtained as the solution to (13), it provides the optimal solution to (12). In this, the beamforming vector $\mathbf{w}_k$ can be derived from the rank-one solutions $\mathbf{W}_k$ of $\mathbf{w}_k = \sqrt{e_k}\mathbf{v}_k$, where e_k and $\mathbf{v}_k$ denote the maximum eigenvalue and the corresponding eigenvector, respectively.

Algorithm 1 Bisection algorithm for solving problem (8)

Input: $t_{\min}=0$; $t_{\max}=\frac{P_{\text{total}}|\mathbf{h}_K|^2}{\sigma_n^2}$; Minimum tolerance μ

1: Initialize $t=(t_{\min}+t_{\max})/2$

2: **repeat**

3: Solve the following problem for t to obtain feasible $\mathbf{W}$

$$\begin{aligned}
&\min_{\mathbf{W}\in\mathbb{C}^{N\times N}} \ \sum_{k=1}^{K}\text{Tr}(\mathbf{W}_k)\\
&\text{s.t. } \text{Tr}(\mathbf{H}_l\mathbf{W}_k)-t(\sum_{i=k+1}^{K}\text{Tr}(\mathbf{H}_l\mathbf{W}_i)+\sigma_n^2)\geq 0,\\
&\qquad\qquad \forall k\in\mathcal{K},\ l=k,k+1,\cdots,K,\\
&\quad \mathbf{W}_k=\mathbf{W}_k^H,\ \mathbf{W}_k\succeq 0,\\
&\quad \sum_{k=1}^{K}\text{Tr}(\mathbf{W}_k)\leq P_{\text{total}},\\
&\quad \sum_{k=1}^{K}\text{Tr}(\mathbf{A}_m\mathbf{W}_k)\geq P_s,\ \forall m\in\mathcal{M},\\
&\quad |\sum_{k=1}^{K}\text{Tr}((\mathbf{A}_p-\mathbf{A}_m)\mathbf{W}_k))|\leq P_{\text{diff}},\\
&\quad \overline{C}\leq\xi.
\end{aligned}\tag{13}$$

4: **if** (13) is feasible

5: $t_{\min}=t$; $t^{\text{opt}}=t$; $\mathbf{W}^{\text{opt}}=\mathbf{W}$

6: **else**

7: $t_{\max}=t$

8: **end if**

9: **until** $(t_{\max}-t_{\min}\leq\mu)$

Output: Optimal value $\mathbf{W}^{\text{opt}}$, t^{opt}

Alternatively, when the rank-one condition is not met, a randomization method can be applied to construct a set of rank-one solutions [39], [40]. Furthermore, [41] proposed a way that is beneficial in creating a rank-one solution without performance loss in Theorem 1.

IV. Robust Beamforming Design in Power Minimization Problem

In the previous section, it was assumed that the considered NOMA-ISAC system has perfect CSI. However, in practical scenarios, the channel estimation and quantization errors make it impossible to achieve perfect CSI at the transmitter [42]–[45]. To overcome these channel uncertainties under imperfect CSI conditions, we explore the robust beamforming design in the NOMA-ISAC system using a worst-case performance optimization methodology. Specifically, we consider the norm-bounded channel uncertainty in this design as follows:

$$\mathbf{h}_l=\hat{\mathbf{h}}_l+\Delta\hat{\mathbf{h}}_l,\tag{14}$$

where $\hat{\mathbf{h}}_l$ and $\Delta\hat{\mathbf{h}}_l$ represent the estimate of the actual channel vector $\mathbf{h}_l$ and the norm-bounded channel estimation error, respectively. We assume that the worst-case channel estimation error is bounded by the error bound threshold $\epsilon\geq 0$. Therefore, (14) should be allowed by the following constraints:

$$\left\|\Delta\hat{\mathbf{h}}_l\right\|_2=\left\|\mathbf{h}_l-\hat{\mathbf{h}}_l\right\|_2\leq\epsilon\ \leftrightarrow\ \Delta\hat{\mathbf{h}}_l^H\mathbf{I}\Delta\hat{\mathbf{h}}_l-\epsilon^2\leq 0,\tag{15}$$

where $\mathbf{I}\in\mathbb{C}^{N\times N}$ is the identity matrix.

Based on the channel ordering presented in (3) and the norm-bounded channel uncertainty defined in (14), the received signal at user l for detecting user k can be expressed as follows:

$$\begin{aligned}
y_l^k=\mathbf{h}_l^H\mathbf{w}_k+\sum_{i=1}^{k-1}\Delta\hat{\mathbf{h}}_l\mathbf{w}_i+\sum_{i=k+1}^{K}\mathbf{h}_l^H\mathbf{w}_i+n_l,\\
\forall k\in\mathcal{K},\ l=k,k+1,\cdots,K,
\end{aligned}\tag{16}$$

where the first term represents the desired signal to be detected, while the second term corresponds to the signal from the previous user 1 to the user $k-1$, which cannot be fully removed due to imperfect CSI at the receiver. The third term is the interference signals from user $k+1$ to user K. Thus, the corresponding SINR of user k at user l is written as:

$$\text{SINR}_l^k=\frac{\mathbf{h}_l^H\mathbf{w}_k\mathbf{w}_k^H\mathbf{h}_l}{\sum\limits_{i=1}^{k-1}\Delta\hat{\mathbf{h}}_l^H\mathbf{w}_i\mathbf{w}_i^H\Delta\hat{\mathbf{h}}_l+\sum\limits_{i=k+1}^{K}\mathbf{h}_l^H\mathbf{w}_i\mathbf{w}_i^H\mathbf{h}_l+\sigma_n^2}.\tag{17}$$

In the following, we focus on a robust beamforming design that ensures the SINR requirement for communication users while sensing targets meet their minimum threshold. Hence, it can be formulated as follows:

$$\begin{aligned}
&\min_{\mathbf{w}_k\in\mathbb{C}^{N\times 1}}\ \sum_{k=1}^{K}\|\mathbf{w}_k\|_2^2\\
&\text{s.t.}\quad \min_{\|\Delta\hat{\mathbf{h}}_l\|^2\leq\epsilon}(\text{SINR}_l^k)\geq\gamma_k^{\min},\ \forall k\in\mathcal{K},&\text{(18a)}\\
&\qquad \Delta\hat{\mathbf{h}}_l^H\mathbf{I}\Delta\hat{\mathbf{h}}_l-\epsilon^2\leq 0,&\text{(18b)}\\
&\qquad \text{(8b)}-\text{(8d)}.
\end{aligned}$$

To solve (18), we employ a similar reformulation approach as used in (12). This allows us to redefine the problem as follows:

$$\begin{aligned}
&\min_{\mathbf{W}\in\mathbb{C}^{N\times N}}\ \sum_{k=1}^{K}\text{Tr}(\mathbf{W}_k)\\
&\text{s.t. }\ \nu_{kl},\ \forall k\in\mathcal{K},\ l=k,k+1,\cdots,K,\\
&\qquad \text{(18b)},\ \text{(12b)},\ \text{(12c)},\ \text{(12e)}-\text{(12g)},
\end{aligned}\tag{19}$$

where ν_{kl} is given as (20) at the top of the next page. However, due to the rank-one constraint (12c) and the uncertainty channel conditions (18b), it is not feasible to obtain the optimal robust beamforming directly. Instead, the rank-one constraints (12c) could be relaxed using SDR, as previously demonstrated.

To mitigate the impact of unknown channel uncertainties in (18b), we reformulated it as a linear matrix by applying the S-procedure technique [42] [43]. The S-procedure is employed to transform two inequalities, (18b) and (20), into a single tractable constraint. This technique is particularly effective for handling channel uncertainty and ensuring worst-case performance guarantees, as it reformulates such constraints

$$
\begin{aligned}
(18a) = & \min_{\|\Delta\hat{\mathbf{h}}_l\|^2 \le \epsilon} (\mathrm{SINR}_l^k) \ge \gamma_k^{\min} \\
= & \frac{(\hat{\mathbf{h}}_l + \Delta\hat{\mathbf{h}}_l)^H \mathbf{W}_k (\hat{\mathbf{h}}_l + \Delta\hat{\mathbf{h}}_l)}{\sum_{i=1}^{k-1} \Delta\hat{\mathbf{h}}_l^H \mathbf{W}_i \Delta\hat{\mathbf{h}}_l + \sum_{i=k+1}^{K} (\hat{\mathbf{h}}_l + \Delta\hat{\mathbf{h}}_l)^H \mathbf{W}_i (\hat{\mathbf{h}}_l + \Delta\hat{\mathbf{h}}_l) + \sigma_n^2} \ge \gamma_k^{\min} \\
= & \Delta\hat{\mathbf{h}}_l^H (\frac{\mathbf{W}_k}{\gamma_k^{\min}} - \sum_{i=k+1}^{K} \mathbf{W}_i - \sum_{i=1}^{k-1} \mathbf{W}_i) \Delta\hat{\mathbf{h}}_l + 2\Re\{(\hat{\mathbf{h}}_l^H (\frac{\mathbf{W}_k}{\gamma_k^{\min}} - \sum_{i=k+1}^{K} \mathbf{W}_i)) \Delta\hat{\mathbf{h}}_l\} + \hat{\mathbf{h}}_l^H (\frac{\mathbf{W}_k}{\gamma_k^{\min}} - \sum_{i=k+1}^{K} \mathbf{W}_i) \hat{\mathbf{h}}_l - \sigma_n^2 \ge 0 \\
= & \nu_{kl}. \qquad (20)
\end{aligned}
$$

into a solvable linear matrix inequality (LMI). In this problem, with the S-procedure, the uncertainty parameters in channel estimation are effectively removed, enabling us to transform the original robust problem into a tractable form while incorporating all possible uncertainty constraints. This transformation facilitates efficient analysis and solution via convex optimization methods. Hence, we apply the S-procedure to combine (18b) and (20) into a single equivalent constraint, expressed as follows:

$$
\mathbf{S}_{kl} = \begin{bmatrix} \mathbf{\Phi} - \sum_{i=1}^{k-1} \mathbf{W}_i + \lambda \mathbf{I} & \mathbf{\Phi}^H \hat{\mathbf{h}}_l \\ \hat{\mathbf{h}}_l^H \mathbf{\Phi} & \hat{\mathbf{h}}_l^H \mathbf{\Phi} \hat{\mathbf{h}}_l - \sigma_n^2 - \lambda \epsilon^2 \end{bmatrix} \succeq 0, \qquad (21)
$$

where $\mathbf{\Phi} = \frac{\mathbf{W}_k}{\gamma_k^{\min}} - \sum_{i=k+1}^{K} \mathbf{W}_i$, and $\lambda \ge 0$, the proof of $\mathbf{S}_{kl}$ is defined in Appendix B.

Lemma 1: The problem in (18) can be reformulated by relaxing the rank-one constraint and utilizing the S-procedure, leading to the following equivalent representation:

$$
\begin{aligned}
& \min_{\mathbf{W} \in \mathbb{C}^{N \times N}} \sum_{k=1}^{K} \mathrm{Tr}(\mathbf{W}_k) \\
& \text{s.t. } \mathbf{W}_k \succeq 0, \ \mathbf{S}_{kl} \succeq 0, \ \forall k \in \mathcal{K}, \ l = k, k+1, \cdots, K, \\
& \quad (12e) - (12g),
\end{aligned} \qquad (22)
$$

where the problem in (22) is feasible, a rank-one optimal solution $\{\mathbf{W}_k^*\}$ is always existent.

Proof: Refer to Appendix C.

For the sensing part, studies [32], [36], and [46] demonstrate that beamforming can be used to express the gain of the sensing beampattern, indicating that (12e) to (12g) only rely on beamforming vectors $\mathbf{w}$ when prior information about the sensing target is available. Thus, if beamforming is used to calculate the requirement of a sensing target, the channel uncertainty will have little impact on the determined requirement.

Considering the above, we claim that, whether the CSI is perfect or imperfect, the equations (12e) to (12g) can be used to perform the requirement for sensing targets [47]. Furthermore, the beamforming algorithm can robustly and efficiently optimize the transmit parameters to meet the requirements of the target under different channel conditions. This ensures that the sensing target receives sufficient beampattern gain to operate reliably regardless of the uncertainties in the channel.

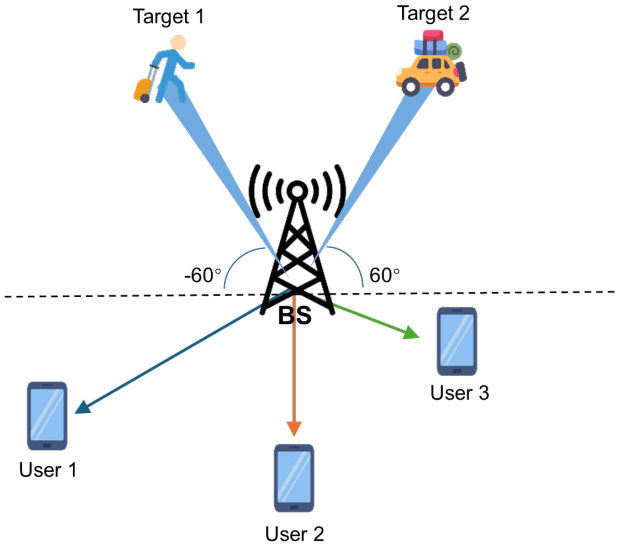

Fig. 2: Simulation of a downlink NOMA-ISAC model.

V. Simulation Results

This section presents simulation results that illustrate the beamforming designs of NOMA in the ISAC system. We consider a NOMA-ISAC system in a single-cell downlink network. The dual-functional BS is equipped with $N = 8$ antennas, serving $K = 3$ communication users and $M = 2$ sensing targets, as shown in Fig. 2. Small-scale fading channels are modeled by Rayleigh fading to represent an isotropic scattering environment. The noise variance for each communication user is assumed to be $\sigma_n^2 = 0.01$, with identical SINR requirements across all users. For the sensing targets, the angles of two sensing targets are $\theta_1 = -60^\circ$ and $\theta_2 = 60^\circ$, with a power differential between them set to $P_{\text{diff}} = 0.001$, and the cross-correlation coefficient specified as $\xi = 10$.

Initially, we analyze the performance of the max-min design for NOMA-ISAC and OMA-ISAC systems under perfect CSI, with the minimum tolerance set to $\mu = 0.02$. Fig. 3 illustrates the performance of the bisection search method by plotting the maximum SINR that communication users achieve the total transmit power, under given the sensing target's power threshold requirement of $P_s = 2$W and $P_s = 3$W, respectively. It is shown that, for a specific transmit power threshold, the NOMA-ISAC system can achieve a higher SINR than the

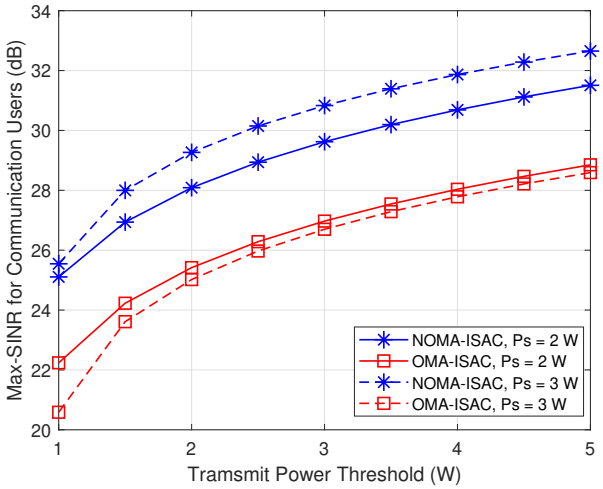

Fig. 3: Achieved max-min SINR versus transmit power in NOMA-ISAC and OMA-ISAC systems with different sensing thresholds.

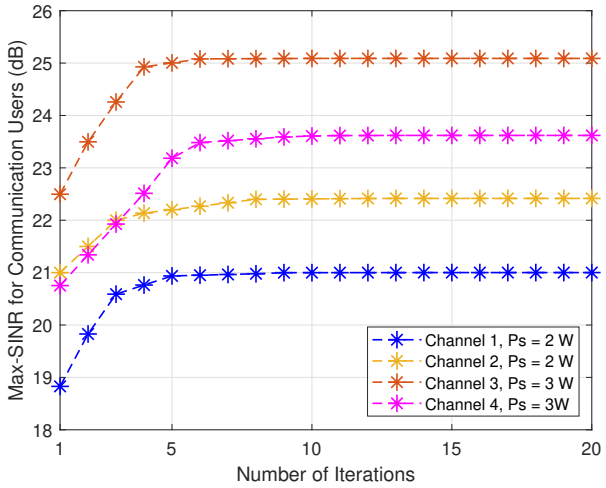

Fig. 4: The convergence of the algorithm in Algorithm 1 for different sets of channels for $P_s = 2$W and $P_s = 3$W in NOMA-ISAC system.

OMA-ISAC system. Additionally, for both NOMA-ISAC and OMA-ISAC systems, increasing the sensing power constraint slightly degrades the communication performance, as more power is reserved for sensing. However, NOMA-ISAC still maintains a clear advantage, even under stricter sensing constraints. This indicates that the ability of NOMA-ISAC to multiplex users and dynamically allocate power effectively improves the SINR performance.

Table I presents the achieved SINR for each communication user and power for each sensing target by solving the problem in (8) across four different random channels for both NOMA-ISAC and OMA-ISAC systems. For both systems, the identical channels are employed in order to allow for a fair comparison. Specifically, it shows that the max-min design provides the same SINR for all communication users while meeting the received sensing power requirements at the sensing targets on different channels in both systems. Notably, under the same channel conditions, the NOMA-ISAC system consistently achieves higher SINR values for all communication users compared to the OMA-ISAC system. This highlights the capability of NOMA-ISAC to utilize the transmit power efficiently. By dynamically adjusting power allocations based on their channel conditions, NOMA-ISAC optimizes transmit power and enhances overall performance in terms of SINRs achieved by communication users and received sensing power at the sensing target performance in the ISAC system.

To verify that the suggested max-min design is optimal, we examine its performance under the same SINR and sensing power thresholds within the same channel by solving the power minimization problem (12) in the NOMA-ISAC system. The results are presented in Table II. Table I and Table II show that the max-min and power minimization designs meet the sensing target requirements, and confirm that the bisection search method employed in Algorithm 1 successfully converges to the optimal solution of the max-min SINR problem. By guaranteeing that each communication user reaches the specific SINR threshold, the power-minimization technique produces an ideal solution and validates the optimality of the suggested max-min design.

In order to confirm Algorithm 1's convergence behavior and optimality, we analyze the relationship between the number of iterations and the resulting maximum SINR for communication users, using the same channel realizations as in Table I under the NOMA-ISAC system. The suggested Algorithm 1 achieves high SINR values and converges rapidly in a limited number of iterations, as illustrated in Fig. 4. This demonstrates that the convergence process is both efficient and computationally tractable, indicating that the algorithm is well-suited for practical implementation.

Next, we evaluate the equivalent proposed power minimization performance based on resource allocation techniques under perfect CSI scenarios in problem (12). Fig. 5 shows the result for this approach given the sensing power thresholds $P_s = 2$W and $P_s = 3$W. In Fig. 5(a), as the SINR threshold increases, the NOMA-ISAC system requires less power to achieve the SINR threshold when compared to the OMA-ISAC system. Fig. 5(b) illustrates the relationship between the total power of sensing for all sensing targets and a given communication SINR threshold. Here, we assume that each sensing target's minimum sensing power threshold is stabilized. As a result, the power allocated to each sensing target remains stable despite the increase in the communication SINR threshold, ensuring that each target's minimum sensing power threshold is always met. Therefore, in the NOMA-ISAC system, communication users can achieve a higher SINR with less transmit power while achieving the minimum power threshold for sensing targets.

Subsequently, as explained in (22), we concentrate on how channel uncertainties affect the total transmit power needed under imperfect CSI. Here, the error bound threshold is set to $\epsilon = 0.05$. The term "Non-robust design" describes a method in which the beamforming vectors are designed based on

TABLE I: Achieved SINRs at the Communication Users and Received Sensing Power at the Sensing Target of the Max-min Design in NOMA-ISAC System and OMA-ISAC System in (8).

Channels (NOMA & OMA)	P_{total} Threshold (W)	P_s Threshold (W)	User 1 SINR (dB)	User 2 SINR (dB)	User 3 SINR (dB)	Target 1 (W)	Target 2 (W)
Channel 1 (NOMA)	1	2	21.0014	21.0014	21.0014	2.0000	2.0000
Channel 1 (OMA)	1	2	19.0942	19.0942	19.0942	2.0000	2.0000
Channel 2 (NOMA)	1.5	2	22.4167	22.4167	22.4167	2.0000	2.0000
Channel 2 (OMA)	1.5	2	20.5510	20.5510	20.5510	2.0000	2.0000
Channel 3 (NOMA)	1.5	3	25.0894	25.0894	25.0894	3.0000	3.0000
Channel 3 (OMA)	1.5	3	23.7835	23.7835	23.7835	3.0000	3.0000
Channel 4 (NOMA)	2	3	23.6193	23.6193	23.6193	3.0000	3.0000
Channel 4 (OMA)	2	3	21.7322	21.7322	21.7322	3.0000	3.0000

TABLE II: SINRs at the Communication Users and Sensing Power at the Sensing Target for a given Communication SINR Threshold through Power Minimization in (12).

Channels (NOMA)	SINR Threshold (dB)	P_s Threshold (W)	User 1 SINR (dB)	User 2 SINR (dB)	User 3 SINR (dB)	Target 1 (W)	Target 2 (W)	P_{total} (W)
Channel 1	21.0014	2	21.0014	21.0014	21.0014	2.0000	2.0000	1
Channel 2	22.4167	2	22.4167	22.4167	22.4167	2.0000	2.0000	1.5
Channel 3	25.0894	3	25.0894	25.0894	25.0894	3.0000	3.0000	1.5
Channel 4	23.6193	3	23.6193	23.6193	23.6193	3.0000	3.0000	2

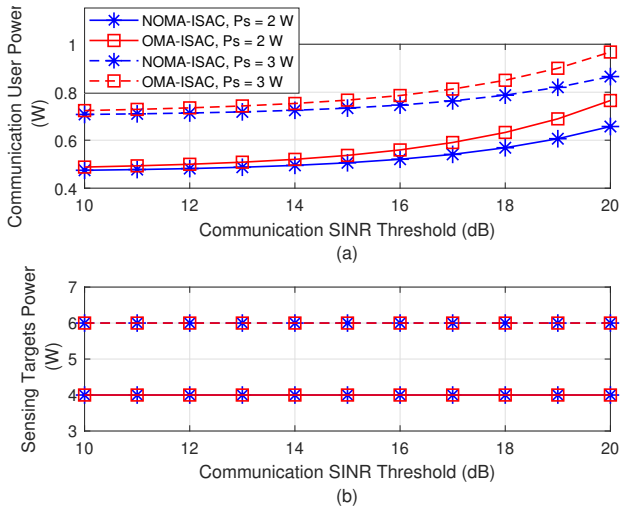

Fig. 5: Achieved power versus SINR in NOMA-ISAC and OMA-ISAC systems.

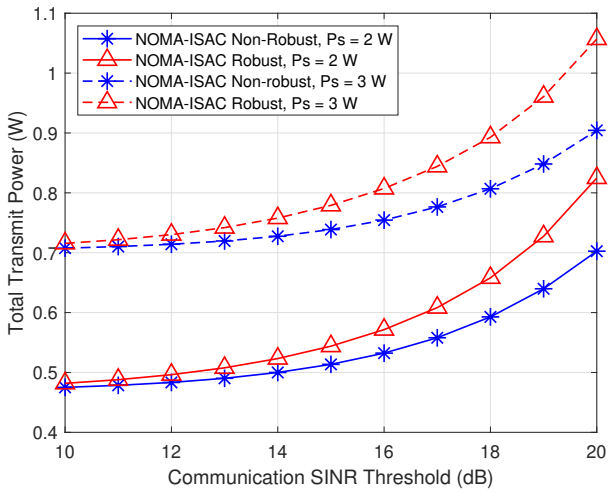

Fig. 6: Achieved total transmit power versus SINR for robust and non-robust design in NOMA-ISAC system.

imperfect CSI, and the BS has no information on channel uncertainty. Fig. 6 compares the total transmit power required for robust and non-robust NOMA-ISAC systems under varying sensing power and communication SINR thresholds, showing that the robust design demands more power as the SINR threshold increases. To investigate the factors contributing to the increased transmit power required by robust design, we analyze how power allocation is affected as the SINR threshold for communication increases. Specifically, the variations in the total power allocated to communication users and target detection are shown in Fig. 7.

Fig. 7(a) illustrates that the robust design requires more power than the non-robust design, while Fig. 7(b) shows that the sensing power could achieve a minimum power threshold for both robust and non-robust designs. This is due to the assumption that the system has the same sensing power threshold for all SINR thresholds, ensuring that sensing targets meet the minimum required threshold. Thus, despite potential variations in channel conditions and uncertainties in CSI, the robust design employs techniques to ensure that the sensing targets achieve the minimum required power threshold.

Therefore, Fig. 6 and Fig. 7 demonstrate that the robust NOMA design primarily affects the power requirements for the communication part, while the sensing part consistently meets its threshold requirements. Although the non-robust design might require lower transmit power, it could struggle to maintain the required SINR threshold under channel uncertainty. This is because, in order to compensate for the effects of the channel, a higher transmit power is needed to achieve the desired SINR threshold under uncertain channel conditions.

To confirm that the robust NOMA design could always achieve the SINR threshold, we compare the performance of the achieved communication SINR for both robust and non-robust designs in the NOMA-ISAC system, which is shown in Fig. 8. In this, the channel error bound is set to $\epsilon = 0.1$, the sensing threshold is $P_s = 2$W, and the SINR threshold is 20

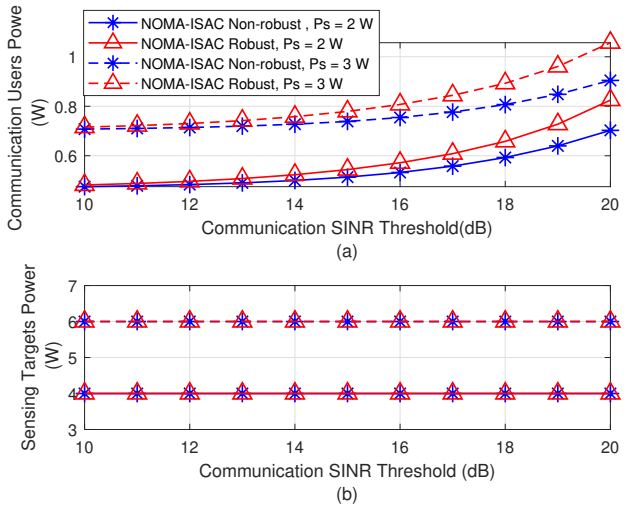

Fig. 7: Achieved power versus SINR for robust and non-robust design in NOMA-ISAC system.

dB for each user. Fig. 8 presents the probability distribution function (PDF) and the cumulative distribution function (CDF) derived from 1,000 random channels. The PDF for the robust design demonstrates that all channels successfully reach the minimum SINR threshold, with the CDF concentrated in a small range, indicating stable performance across channels. On the other hand, the PDF and CDF plots of the non-robust design fall below the required SINR threshold. This suggests that the non-robust design may struggle to achieve satisfactory SINR levels, particularly in scenarios with channel errors or uncertainties.

Therefore, this robust design demonstrates superior performance in achieving and maintaining desired communication SINR thresholds across uncertain channel conditions, making it more suitable for practical use. By considering uncertainties yielded by imperfect CSI, the robust design significantly enhances system resilience and reliability, leading to consistent satisfaction with SINR requirements for communication users while achieving the requirements of the sensing targets.

VI. Conclusions

In this paper, we proposed two beamforming techniques for an ISAC system based on NOMA, referred to as the NOMA-ISAC system. Specifically, two resource allocation problems for this NOMA-ISAC system were considered: the max-min SINR problem under perfect CSI and minimizing the total transmit power problem under imperfect CSI. To solve the original non-convex problem, we developed an iterative algorithm using SDR techniques for the first problem, which is equivalent to solving the minimized total transmit power problem. These analyses indicated that NOMA-ISAC achieves equivalent SINR thresholds while ensuring the requirement of the sensing targets and outperforms OMA-ISAC under perfect CSI. For the second robust design problem, non-convex constraints were transformed into a set of linear matrix forms to enhance system performance under channel uncertainties. The results showed that even in the presence of channel uncertainties, the robust design continuously meets SINR requirements, outperforming the non-robust design for communication users.

The results of this study highlight the significant potential of integrating NOMA into ISAC systems. NOMA overcomes the limitations of traditional OMA technology by multiplexing users in the power domain, greatly increasing spectrum efficiency. The proposed NOMA-ISAC system demonstrates that this integration enhances overall system performance, yielding higher SINR levels for communication users and robust sensing accuracy in both perfect and imperfect CSI scenarios. These improvements establish NOMA as a promising enabling technology for future ISAC systems, providing a scalable and resilient approach to meet both communication and sensing demands. This capability is especially critical for 6G and next-generation wireless networks, which require massive connectivity, ultra-reliable low-latency communication, and high spectral efficiency.

Appendix A: Proof of (13)

To prove that solving (13) without the rank-one constraint can still yield a rank-one solution, indicate that the SDR is tight; it can be considered by analyzing Karush-Kuhn-Tucker (KKT) conditions. First, we write the Lagrangian dual function of (13) as follows:

$$\begin{aligned}
&\mathcal{L}(\mathbf{W}_k, \mathbf{Y}_k, \lambda_{k,l}, \mathbf{D}_m, \mathbf{F}_{pm}, \xi) \\
&= \sum_k \mathrm{Tr}(\mathbf{W}_k) - \sum_{k=1}^{K} \mathrm{Tr}(\mathbf{Y}_k \mathbf{W}_k) \\
&- \sum_{k,l} \lambda_{k,l} \left[\mathrm{Tr}(\mathbf{H}_l \mathbf{W}_k) - t\Big(\sum_{i=k+1}^{K} \mathrm{Tr}(\mathbf{H}_l \mathbf{W}_i) + \sigma_n^2 \Big) \right] \\
&- \eta_k (P_{\text{total}} - \sum_k \mathrm{Tr}(\mathbf{W}_k)) \\
&- \sum_m (\mathbf{D}_m (\sum_k \mathrm{Tr}(\mathbf{A}_m \mathbf{W}_k) - P_s)) \\
&- \sum_{p \neq m} (\mathbf{F}_{pm} (P_{\text{diff}} - \sum_k \mathrm{Tr}\,|(\mathbf{A}_p - \mathbf{A}_m)\mathbf{W}_k|)) \\
&- \mu_{pm} (\xi - \left| \alpha^H(\theta_p) \sum_k (\mathbf{W}_k) \alpha(\theta_m) \right|^2),
\end{aligned} \tag{A.1}$$

where $\mathbf{Y}_k$, $\lambda_{k,l} \geq 0$,$\eta_k \geq 0$, $\mathbf{D}_m$, $\mathbf{F}_{pm}$ and $\mu_{pm} \geq 0$ are the Lagrangian multipliers associated with the respective constraints.

Hence, by deriving the gradient of the $\mathbf{W}_k$, the (A.1) can be rewritten as:

$$\begin{aligned}
\frac{\partial \mathcal{L}}{\partial \mathbf{W}_k} &= \mathbf{G}_k, \\
&= \mathbf{I} - \mathbf{Y}_k - \sum_l \lambda_{k,l} \mathbf{H}_l + \sum_{k<i} t \lambda_{i,l} \mathbf{H}_l \\
&- \eta \mathbf{I} - \sum_m \mathbf{D}_m \mathbf{A}_m - \mathbf{F}_{pm} \mathbf{A}_m - \mathbf{F}_{pm} \mathbf{A}_p \\
&+ \mu_{pm} (\boldsymbol{\alpha}(\theta_p) \boldsymbol{\alpha}^H(\theta_m)).
\end{aligned} \tag{A.2}$$

For the complementary slackness condition, it has:

$$\mathbf{G}_k + \mathbf{Y}_k = 0, \quad \text{with} \quad \mathbf{Y}_k \succeq 0,\ \mathbf{Y}_k \mathbf{W}_k = 0. \tag{A.3}$$

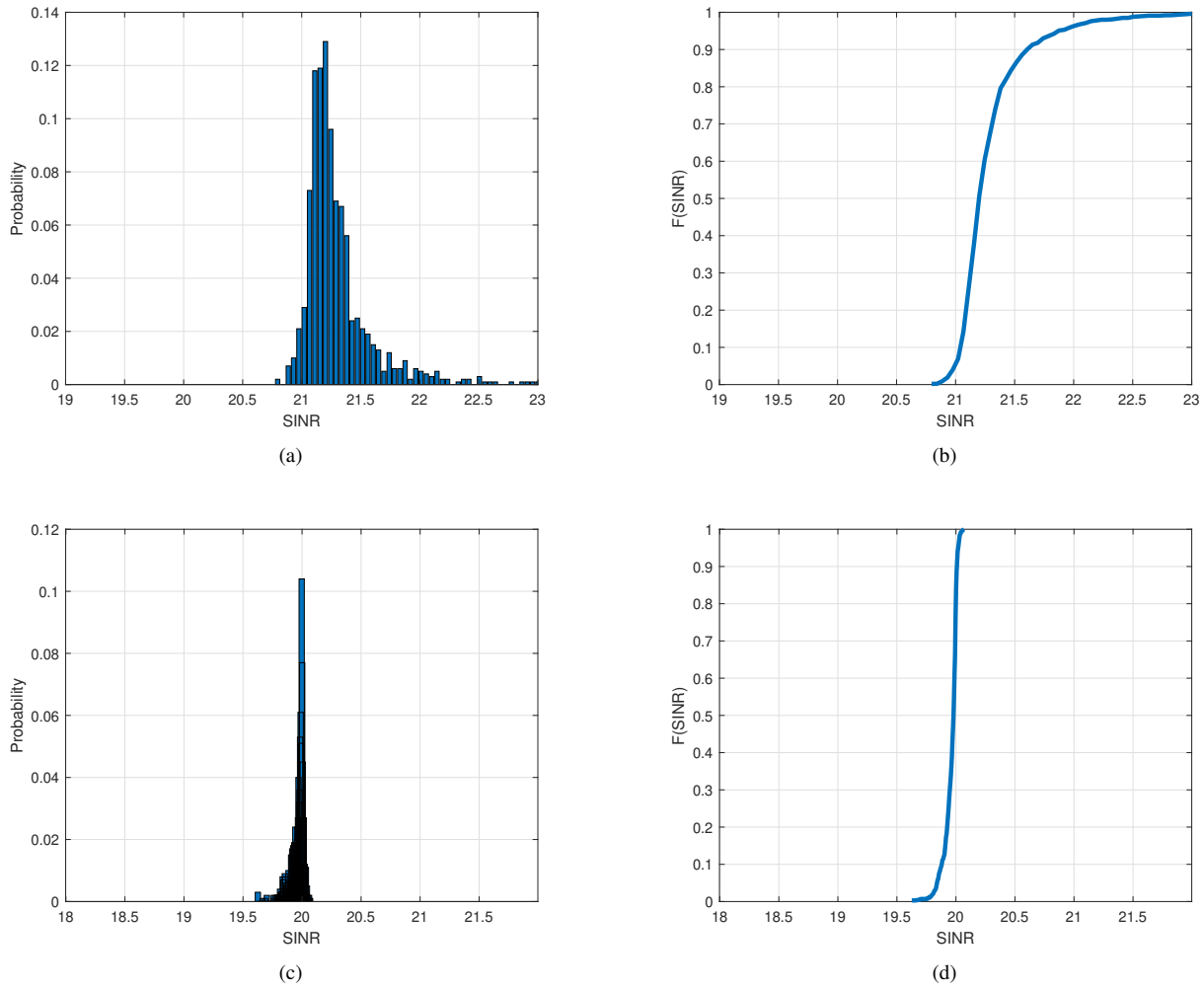

Fig. 8: Comparison PDF and CDF of minimum achieved SINR for robust and non-robust design in NOMA-ISAC system. (a) Robust design PDF. (b) Robust design CDF. (c) Non-robust design PDF. (D) Non-robust design CDF.

From the $\mathbf{Y}_k\mathbf{W}_k = 0$, it follows that the range space of $\mathbf{W}_k$ is contained within the null space of the dual matrix $\mathbf{Y}_k$. If $\mathbf{Y}_k$ has only one eigenvalue, then the null space is one-dimensional, implying that rank $(\mathbf{W}_k) \leq 1$.

To access the rank structure of $\mathbf{Y}_k$, we consider its composition. The matrix $\mathbf{G}_k$, which contributes directly to $\mathbf{Y}_k$, includes the identity matrix $\mathbf{I}$, which is of full rank, along with a sum of other terms such as $\mathbf{H}_l$, $\mathbf{A}_m$, and $\mathbf{A}_p$, all predefined as rank-one. Furthermore, $\boldsymbol{\alpha}(\theta_p)\boldsymbol{\alpha}^H(\theta_m)$ is also rank-one. Hence, $\mathbf{G}_k$ can be interpreted as a Hermitian matrix composed of a full-rank component plus a linear combination of rank-one matrices, which means that the $\mathbf{G}_k$ has:

$$\text{null}(\mathbf{G}_k) \leq 1 \Rightarrow \text{rank}(\mathbf{W}_k) \leq 1, \tag{A.4}$$

where in (12b), it defines that $\mathbf{W}_k \succeq 0$, which means that the eigenvalues of $\mathbf{W}_k$ should be either zero or positive. Based on this, we conclude that:

$$\text{rank}(\mathbf{W}_k) = 1. \tag{A.5}$$

Appendix B: Proof of (21)

First assume that $f_j(\mathbf{x}), j = 1, 2$ and define:

$$\begin{aligned} f_1(\mathbf{x}) &= \mathbf{x}^H\mathbf{B}_1\mathbf{x} + 2\Re\{\mathbf{c}_1^H\mathbf{x}\} + q_1 \geq 0, \\ f_2(\mathbf{x}) &= \mathbf{x}^H\mathbf{B}_2\mathbf{x} + 2\Re\{\mathbf{c}_2^H\mathbf{x}\} + q_2 \geq 0. \end{aligned} \tag{B.1}$$

where $\mathbf{B}_j = \mathbf{B}_j^H \in \mathbb{C}^{N\times N}$, $\mathbf{c}_j \in \mathbb{C}^{N\times 1}$ and $q_j \in \mathbb{R}$. If there exists $\hat{\mathbf{x}}$ to provide $f_1(\hat{\mathbf{x}}) > 0$, then it should have and only have one $\lambda \geq 0$ to implement $f_1(\mathbf{x}) \geq 0 \Rightarrow f_2(\mathbf{x}) \geq 0$, which can written in the following linear matrix inequality:

$$\begin{bmatrix} \mathbf{B}_2 - \lambda\mathbf{B}_1 & \mathbf{c}_2 - \lambda\mathbf{c}_1 \\ \mathbf{c}_2^H - \lambda\mathbf{c}_1^H & q_2 - \lambda q_1 \end{bmatrix} \succeq 0. \tag{B.2}$$

For (20), we assume that $\boldsymbol{\Phi} = \frac{\mathbf{W}_k}{\gamma_k^{\min}} - \sum_{i=k+1}^{K}\mathbf{W}_i$, hence, (20) can be expressed as follow:

$$\begin{aligned} \nu_{kl} = \Delta\hat{\mathbf{h}}_l^H(\boldsymbol{\Phi} - \sum_{i=1}^{k-1}\mathbf{W}_i)\Delta\hat{\mathbf{h}}_l + 2\Re\{(\hat{\mathbf{h}}_l^H\boldsymbol{\Phi})\Delta\hat{\mathbf{h}}_l\} \\ +\hat{\mathbf{h}}_l^H\boldsymbol{\Phi}\hat{\mathbf{h}}_l - \sigma_n^2 \geq 0. \end{aligned} \tag{B.3}$$

Meanwhile, (18b) with the express of $\mathbf{B}_1$, $\mathbf{c}_1$, $\mathbf{c}_1^H$ and q_1 is give as follow:

$$f_1(\Delta\hat{\mathbf{h}}_l) = \begin{cases} \mathbf{B}_1 = \mathbf{I}, \\ \mathbf{c}_1 = 0, \\ \mathbf{c}_1^H = 0, \\ q_1 = \epsilon^2. \end{cases} \tag{B.4}$$

Additionally, (B.3) with the form $\mathbf{B}_2$, $\mathbf{c}_2$, $\mathbf{c}_2^H$, and q_2 is given as follow:

$$f_2(\Delta\hat{\mathbf{h}}_l) = \begin{cases} \mathbf{B}_2 = \mathbf{\Phi} - \sum_{i=1}^{k-1} \mathbf{W}_i, \\ \mathbf{c}_2 = \mathbf{\Phi}^H \hat{\mathbf{h}}_l, \\ \mathbf{c}_2^H = \mathbf{\Phi}\hat{\mathbf{h}}_l^H, \\ q_2 = \hat{\mathbf{h}}_l^H \mathbf{\Phi} \hat{\mathbf{h}}_l - \sigma_n^2. \end{cases} \tag{B.5}$$

Replacing (B.4) and (B.5), and replacing into (B.1), the following linear matrix inequality can be written as:

$$\mathbf{S}_{kl} = \begin{bmatrix} \mathbf{\Phi} - \sum_{i=1}^{k-1} \mathbf{W}_i + \lambda \mathbf{I} & \mathbf{\Phi}^H \hat{\mathbf{h}}_l \\ \hat{\mathbf{h}}_l^H \mathbf{\Phi} & \hat{\mathbf{h}}_l^H \mathbf{\Phi} \hat{\mathbf{h}}_l - \sigma_n^2 - \lambda\epsilon^2 \end{bmatrix} \succeq 0. \tag{B.6}$$

Appendix C: Proof of (22)

The Karush-Kuhn-Tucker (KKT) conditions are examined to prove (22). First, we write the Lagrangian dual function of (22) as follows:

$$\begin{aligned} &\mathcal{L}(\mathbf{W}_k, \mathbf{Y}_k, \lambda, \mathbf{T}_{kl}, \mathbf{D}_m, \mathbf{F}_{pm}, \mu_{pm}) \\ &= \sum_k \mathrm{Tr}(\mathbf{W}_k) - \sum_k \mathrm{Tr}(\mathbf{Y}_k \mathbf{W}_k) \\ &- \sum_{kl} \mathrm{Tr}(\mathbf{T}_{kl}\mathbf{C}_1) - \sum_{kl} \mathrm{Tr}[\mathbf{T}_{kl}\mathbf{H}_l^H \mathbf{\Phi} \mathbf{H}_l] - \sum_{kl} \mathrm{Tr}(\mathbf{T}_{kl}\mathbf{C}_2) \\ &- \sum_m (\mathbf{D}_m (\sum_k \mathrm{Tr}(\mathbf{A}_m \mathbf{W}_k) - P_s)) \\ &- \sum_{p \neq m} (\mathbf{F}_{pm} (P_{\text{diff}} - \sum_k \mathrm{Tr}\,|(\mathbf{A}_p - \mathbf{A}_m)\mathbf{W}_k|)) \\ &- \mu_{pm} (\xi - \left| \alpha^H(\theta_p) \sum_k (\mathbf{W}_k) \alpha(\theta_m) \right|^2), \end{aligned} \tag{C.1}$$

where $\mathbf{Y}_k$, $\mathbf{T}_{kl}$, $\mathbf{D}_m$ and $\mathbf{F}_{pm}$ are the Lagrangian multipliers associated with the respective constraints, and μ_{pm} is a Lagrangian multiplier for the constraint (12g).

The $\mathbf{H}_l$ is defined as $\mathbf{H}_l = [\mathbf{I} \quad \mathbf{h}_l]$, and $\mathbf{C}_1$ and $\mathbf{C}_2 =$ are given as:

$$\mathbf{C}_1 = \begin{bmatrix} \lambda \mathbf{I} & \mathbf{0} \\ \mathbf{0} & -\sigma_n^2 - \lambda\epsilon^2 \end{bmatrix}, \mathbf{C}_2 = \begin{bmatrix} -\sum_{i=1}^{k-1} \mathbf{W}_i & \mathbf{0} \\ \mathbf{0} & 0 \end{bmatrix}. \tag{C.2}$$

Hence, the following KKT condition for (C.1) is given as:

$$\begin{aligned} \frac{\partial \mathcal{L}}{\partial \mathbf{W}_k} &= \mathbf{0}, \\ &= \mathbf{I} - \mathbf{Y}_k - (\mathbf{H}_l \mathbf{T}_{kl} \mathbf{H}_l^H)/\gamma_k^{\min} \\ &- \sum_m \mathbf{D}_m \mathbf{A}_m - \mathbf{F}_{pm}\mathbf{A}_m - \mathbf{F}_{pm}\mathbf{A}_p \\ &+ \mu_{pm}(\boldsymbol{\alpha}(\theta_p)\boldsymbol{\alpha}^H(\theta_m)), \quad \forall k = 1, 2, \ldots, K. \end{aligned} \tag{C.3}$$

In Appendix A, it confirms that the rank of $\mathbf{A}_m$, $\mathbf{A}_p$ and $\boldsymbol{\alpha}(\theta_p)\boldsymbol{\alpha}^H(\theta_m)$ is rank-one. Additionally, the dual feasibility of (C.3) should also be satisfied by the following:

$$\mathbf{Y}_k \mathbf{W}_k = \mathbf{0}, \ \forall k = 1, 2, \ldots, K, \tag{C.4a}$$

$$(\mathbf{C}_1 + \mathbf{H}_l^H \mathbf{\Phi} \mathbf{H}_l + \mathbf{C}_2)\mathbf{T}_{kl} = \mathbf{0}, \ \forall k = 1, 2, \ldots, K, \tag{C.4b}$$

where $\mathbf{\Phi} = \frac{\mathbf{W}_k}{\gamma_k^{\min}} - \sum_{i=k+1}^{K} \mathbf{W}_i$.

Then, following the rank relation, we can write the rank constraint as:

$$\begin{aligned} \mathrm{rank}(\mathbf{W}_k) &= \mathrm{rank}[\mathbf{W}_k(\mathbf{I} + (\mathbf{H}_l \mathbf{T}_{kl} \mathbf{H}_l^H)] \\ &\leq \min\left\{\mathrm{rank}(\mathbf{H}_l \mathbf{T}_{kl} \mathbf{H}_l^H), \mathrm{rank}(\mathbf{W}_k)\right\}, \end{aligned} \tag{C.5}$$

therefore, if $\mathrm{rank}(\mathbf{W}_k) \leq 1$, it is necessary to show that $\mathrm{rank}(\mathbf{H}_l \mathbf{T}_{kl} \mathbf{H}_l^H) \leq 1$.

To proof the $\mathrm{rank}(\mathbf{W}_k) \leq 1$, we first consider pre-multiply $[\mathbf{I} \quad \mathbf{0}]$ and post-multiply $\mathbf{H}_l^H$ for (C.4b), which is given as:

$$[\mathbf{I} \quad \mathbf{0}]\,(\mathbf{C}_1 + \mathbf{H}_l^H \mathbf{\Phi} \mathbf{H}_l + \mathbf{C}_2)\mathbf{T}_{kl}\mathbf{H}_l^H \tag{C.6a}$$

$$= \lambda(\mathbf{H}_l - [\mathbf{0} \quad \mathbf{h}_l])\mathbf{T}_{kl}\mathbf{H}_l^H \tag{C.6b}$$

$$+ \mathbf{\Phi}\mathbf{H}_l\mathbf{T}_{kl}\mathbf{H}_l^H + (-\sum_{i=1}^{k-1}\mathbf{W}_i)(\mathbf{H}_l - [\mathbf{0} \quad \mathbf{h}_l])\mathbf{T}_{kl}\mathbf{H}_l^H \tag{C.6c}$$

$$= (\lambda\mathbf{I} + \mathbf{\Phi} - \sum_{i=1}^{k-1}\mathbf{W}_i)\mathbf{H}_l\mathbf{T}_{kl}\mathbf{H}_l^H \tag{C.6d}$$

$$- (\lambda\mathbf{I} - \sum_{i=1}^{k-1}\mathbf{W}_i)\,[\mathbf{0} \quad \mathbf{h}_l]\,\mathbf{T}_{kl}\mathbf{H}_l^H \tag{C.6e}$$

$$= \mathbf{0}. \tag{C.6f}$$

It can be seen that in (C.6e), the matrix $(\lambda\mathbf{I} + \mathbf{\Phi} - \sum_{i=1}^{k-1}\mathbf{W}_i)$ is same as the linear matrix $\mathbf{S}_{kl}$ which given as (B.6).

It is known that if a block Hermitian matrix $\mathbf{C} = \begin{bmatrix} \mathbf{C}_1 & \mathbf{C}_2 \\ \mathbf{C}_3 & \mathbf{C}_4 \end{bmatrix} \succeq \mathbf{0}$ then the main diagonal matrices $\mathbf{C_1}$ and $\mathbf{C_4}$ must be positive definite matrix [48]. Hence, the matrix $(\lambda\mathbf{I} + \mathbf{\Phi} - \sum_{i=1}^{k-1}\mathbf{W}_i)$ that represents $\mathbf{C_1}$ in (B.6) is positive and nonsingular, and multiplying by a nonsingular matrix will not change the rank of the matrix. In addition, the first and the second part of (C.6e) have the same dimensions; if the first part does not influence the rank, only the second part will influence the rank. Thus, the following rank relation holds:

$$\begin{aligned} \mathrm{rank}(\mathbf{H}_l\mathbf{T}_{kl}\mathbf{H}_l^H) &= \mathrm{rank}\left((\lambda\mathbf{I} - \sum_{i=1}^{k-1}\mathbf{W}_i)\,[\mathbf{0} \quad \mathbf{h}_l]\,\mathbf{T}_{kl}\mathbf{H}_l^H\right) \\ &\leq \mathrm{rank}([\mathbf{0} \quad \mathbf{h}_l] \\ &\leq 1. \end{aligned} \tag{C.7}$$

This completes the proof of *Lemma 1*.

References

[1] F. Liu, Y. Cui, C. Masouros, J. Xu, T. X. Han, Y. C. Eldar, and S. Buzzi, "Integrated Sensing and Communications: Toward dual-functional wireless networks for 6G and beyond," *IEEE J. Sel. Areas Commun.*, vol. 40, no. 6, pp. 1728–1767, Aug. 2022.

[2] S. R. Islam, N. Avazov, O. A. Dobre, and K.-S. Kwak, "Power-domain non-orthogonal multiple access (NOMA) in 5G systems: Potentials and challenges," *IEEE Commun. Surveys Tuts.*, vol. 19, no. 2, pp. 721–742, Oct. 2016.

[3] J. Choi, "NOMA: Principles and recent results," in *Proc. Int. Symp. Wireless. Commun. Syst.*, Bologna, Italy, 2017, pp. 349–354.

[4] Y. Liu, S. Zhang, X. Mu, Z. Ding, R. Schober, N. Al-Dhahir, E. Hossain, and X. Shen, "Evolution of NOMA toward next generation multiple access (NGMA) for 6G," *IEEE J. Sel. Areas Commun.*, vol. 40, no. 4, pp. 1037–1071, Apr. 2022.

[5] G. N. Saddik, R. S. Singh, and E. R. Brown, "Ultra-wideband multifunctional communications/radar system," *IEEE Trans. Microwave Theory Tech.*, vol. 55, no. 7, pp. 1431–1437, Jul. 2007.

[6] M. Jamil, H.-J. Zepernick, and M. I. Pettersson, "On integrated radar and communication systems using oppermann sequences," in *IEEE Military Commun.Conf.*, San Diego, California., Nov. 2008, pp. 1–6.

[7] L. Han and K. Wu, "Joint wireless communication and radar sensing systems–state of the art and future prospects," *IET MICROW ANTENNA P.*, vol. 7, no. 11, pp. 876–885, Aug. 2013.

[8] J. A. Zhang, M. L. Rahman, K. Wu, X. Huang, Y. J. Guo, S. Chen, and J. Yuan, "Enabling joint communication and radar sensing in mobile networks—A survey," *IEEE Commun. Surveys Tuts.*, vol. 24, no. 1, pp. 306–345, Oct. 2021.

[9] W. Saad, M. Bennis, and M. Chen, "A vision of 6g wireless systems: Applications, trends, technologies, and open research problems," *IEEE network*, vol. 34, no. 3, pp. 134–142, Oct. 2019.

[10] R. W. Heath, N. Gonzalez-Prelcic, S. Rangan, W. Roh, and A. M. Sayeed, "An overview of signal processing techniques for millimeter wave MIMO systems," *IEEE J. Sel. Top. Signal Process*, vol. 10, no. 3, pp. 436–453, Feb. 2016.

[11] C. Sturm and W. Wiesbeck, "Waveform design and signal processing aspects for fusion of wireless communications and radar sensing," *IEEE Proc.*, vol. 99, no. 7, pp. 1236–1259, Jul. 2011.

[12] F. Liu, C. Masouros, A. Li, H. Sun, and L. Hanzo, "MU-MIMO communications with MIMO radar: From co-existence to joint transmission," *IEEE Trans. Wireless Commun.*, vol. 17, no. 4, pp. 2755–2770, Apr. 2018.

[13] F. Liu, C. Masouros, A. P. Petropulu, H. Griffiths, and L. Hanzo, "Joint radar and communication design: Applications, state-of-the-art, and the road ahead," *IEEE Trans. Commun.*, vol. 68, no. 6, pp. 3834–3862, Jun. 2020.

[14] X. Liu, T. Huang, N. Shlezinger, Y. Liu, J. Zhou, and Y. C. Eldar, "Joint transmit beamforming for multiuser MIMO communications and MIMO radar," *IEEE Trans. Sig. Process.*, vol. 68, pp. 3929–3944, Jun. 2020.

[15] F. Dong, W. Wang, Z. Hu, and T. Hui, "Low-complexity beamformer design for joint radar and communications systems," *IEEE Commun. Lett.*, vol. 25, no. 1, pp. 259–263, Jan. 2020.

[16] J. Wang, N. Varshney, C. Gentile, S. Blandino, J. Chuang, and N. Golmie, "Integrated Sensing and Communication: Enabling Techniques, Applications, Tools and Data Sets, Standardization, and Future Directions," *IEEE IoT J.*, vol. 9, no. 23, pp. 23 416–23 440, Dec. 2022.

[17] Z. Wei, F. Liu, C. Masouros, N. Su, and A. P. Petropulu, "Toward Multi-Functional 6G Wireless Networks: Integrating Sensing, Communication, and Security," *IEEE Commun. Mag.*, vol. 60, no. 4, pp. 65–71, Apr. 2022.

[18] H. Hua, J. Xu, and T. X. Han, "Optimal transmit beamforming for integrated sensing and communication," *IEEE Trans. Veh. Technol.*, Mar. 2023.

[19] A. Bayesteh, J. He, Y. Chen, P. Zhu, J. Ma, A. Shaban, Z. Yu, Y. Zhang, Z. Zhou, and G. Wang, "Integrated sensing and communication (ISAC)—From concept to practice," *Communications of Huawei Research*, pp. 4–25, 2022.

[20] J. Ye, L. Huang, Z. Chen, P. Zhang, and M. Rihan, "Unsupervised learning for joint beamforming design in RIS-aided ISAC systems," *IEEE Wireless Commun. Lett.*, May. 2024.

[21] C. Liu, W. Yuan, S. Li, X. Liu, H. Li, D. W. K. Ng, and Y. Li, "Learning-based predictive beamforming for integrated sensing and communication in vehicular networks," *IEEE J. Sel. Areas Commun.*, vol. 40, no. 8, pp. 2317–2334, Jun. 2022.

[22] W. Jiang, D. Ma, Z. Wei, Z. Feng, P. Zhang, and J. Peng, "ISAC-NET: Model-driven deep learning for integrated passive sensing and communication," *IEEE Trans. Commun.*, Mar. 2024.

[23] W. Xu, Z. Yang, D. W. K. Ng, M. Levorato, Y. C. Eldar, and M. Debbah, "Edge learning for B5G networks with distributed signal processing: Semantic communication, edge computing, and wireless sensing," *IEEE J. Sel. Top. Signal Process*, vol. 17, no. 1, pp. 9–39, Jan. 2023.

[24] L. Dai, B. Wang, Y. Yuan, S. Han, I. Chih-Lin, and Z. Wang, "Non-orthogonal multiple access for 5G: solutions, challenges, opportunities, and future research trends," *IEEE Commun. Mag.*, vol. 53, no. 9, pp. 74–81, Sept. 2015.

[25] Y. Liu, Z. Qin, M. Elkashlan, Z. Ding, A. Nallanathan, and L. Hanzo, "Nonorthogonal multiple access for 5G and beyond," *IEEE Proc.*, vol. 105, no. 12, pp. 2347–2381, Dec. 2017.

[26] T. Cover, "Broadcast channels," *IEEE Trans. Inf. Theory*, vol. 18, no. 1, pp. 2–14, Jan. 1972.

[27] Q. C. Li, H. Niu, A. T. Papathanassiou, and G. Wu, "5G network capacity: Key elements and technologies," *IEEE Veh. Technol. Mag.*, vol. 9, no. 1, pp. 71–78, Mar. 2014.

[28] P. Xu and K. Cumanan, "Optimal power allocation scheme for non-orthogonal multiple access with $\backslash\alpha$-fairness," *IEEE J. Sel. Areas Commun.*, vol. 35, no. 10, pp. 2357–2369, Oct. 2017.

[29] F. Alavi, K. Cumanan, M. Fozooni, Z. Ding, S. Lambotharan, and O. A. Dobre, "Robust energy-efficient design for MISO non-orthogonal multiple access systems," *IEEE Trans. Commun*, vol. 67, no. 11, pp. 7937–7949, Jul. 2019.

[30] X. Mu, Z. Wang, and Y. Liu, "NOMA for integrating sensing and communications towards 6G: A multiple access perspective," *IEEE Wireless Commun.*, Jan. 2023.

[31] X. Huang, G. Zhang, D. Wang, H. Xu, Y. Chen, and R. Li, "Outage constrained transmission design for NOMA-based integrated sensing and communication systems," *Physical Communication*, vol. 63, p. 102292, Apr. 2024.

[32] Z. Wang, Y. Liu, X. Mu, Z. Ding, and O. A. Dobre, "NOMA empowered integrated sensing and communication," *IEEE Commun. Lett.*, vol. 26, no. 3, pp. 677–681, Mar. 2022.

[33] B. Zhao, C. Ouyang, X. Zhang, and Y. Liu, "Downlink and uplink NOMA-ISAC with signal alignment," *IEEE Trans. Wireless Commun.*, Jul 2024.

[34] C. Ouyang, Y. Liu, and H. Yang, "Revealing the impact of SIC in NOMA-ISAC," *IEEE Wireless Commun. Lett.*, Oct. 2023.

[35] M. F. Hanif, Z. Ding, T. Ratnarajah, and G. K. Karagiannidis, "A minorization-maximization method for optimizing sum rate in the downlink of non-orthogonal multiple access systems," *IEEE Trans. Sig. Process.*, vol. 64, no. 1, pp. 76–88, Jan. 2016.

[36] P. Stoica, J. Li, and Y. Xie, "On probing signal design for MIMO radar," *IEEE Trans. Sig. Process.*, vol. 55, no. 8, pp. 4151–4161, 2007.

[37] M. Bengtsson and B. Ottersten, "Optimal downlink beamformingusing semidefinite optimization," in *Annual. Allerton. Conf. Commun. Control Comput.*, 1999, pp. 987–996.

[38] Z.-Q. Luo, W.-K. Ma, A. M.-C. So, Y. Ye, and S. Zhang, "Semidefinite relaxation of quadratic optimization problems," *IEEE Sig. Process. Mag.*, vol. 27, no. 3, pp. 20–34, Apr. 2010.

[39] S. Nasseri and M. R. Nakhai, "Robust interference management via outage-constrained downlink beamforming in multicell networks," in *Proc. IEEE Global. Commun. Conf. GLOBECOM*, Atlanta, Georgia, USA., Dec. 2013, pp. 3470–3475.

[40] H. Dahrouj and W. Yu, "Coordinated beamforming for the multicell multi-antenna wireless system," *IEEE Trans. Wireless Commun.*, vol. 9, no. 5, pp. 1748–1759, May. 2010.

[41] Z. He, W. Xu, H. Shen, D. W. K. Ng, Y. C. Eldar, and X. You, "Full-duplex communication for ISAC: Joint beamforming and power optimization," *IEEE J. Sel. Areas Commun.*, vol. 41, no. 9, pp. 2920–2936, Jun. 2023.

[42] F. Alavi, K. Cumanan, Z. Ding, and A. G. Burr, "Robust beamforming techniques for non-orthogonal multiple access systems with bounded channel uncertainties," *IEEE Commun. Lett.*, vol. 21, no. 9, pp. 2033–2036, Sept. 2017.

[43] K. Cumanan, Z. Ding, B. Sharif, G. Y. Tian, and K. K. Leung, "Secrecy rate optimizations for a MIMO secrecy channel with a multiple-antenna eavesdropper," *IEEE Trans. Veh. Technol.*, vol. 63, no. 4, pp. 1678–1690, May. 2014.

[44] A. Waraiet, K. Cumanan, Z. Ding, and O. A. Dobre, "Robust design for IRS-assisted MISO-NOMA systems: A DRL-based approach," *IEEE Wireless Commun. Lett.*, vol. 13, no. 3, pp. 592–596, Nov. 2023.

[45] K. Cumanan, Z. Ding, Y. Rahulamathavan, M. M. Molu, and H.-H. Chen, "Robust MMSE beamforming for multiantenna relay networks," *IEEE Trans. Veh. Technol.*, vol. 66, no. 5, pp. 3900–3912, May. 2016.

[46] R. Li, Z. Xiao, and Y. Zeng, "Beamforming Towards Seamless Sensing Coverage for Cellular Integrated Sensing and Communication," in *Proc. IEEE Int. Conf. Commun. Workshops*, Seoul, South Korea, May. 2022, pp. 492–497.

[47] Z. Ren, L. Qiu, J. Xu, and D. W. K. Ng, "Robust transmit beamforming for secure integrated sensing and communication," *IEEE Trans. Commun.*, vol. 71, no. 9, pp. 5549–5564, Sept. 2023.

[48] X. Zhang, *Matrix analysis and applications*. Cambridge University Press, Oct. 2017.